

Big Bang Nucleosynthesis: an accurate determination of light element yields

S. Esposito, G. Mangano, G. Miele, and O. Pisanti,

Dipartimento di Fisica, Università di Napoli "Federico II", and INFN, Sezione di Napoli, Mostra D'Oltremare Pad. 20, I-80125 Napoli, Italy

Abstract

We report the results of a new accurate evaluation of light nuclei yields in primordial nucleosynthesis. All radiative effects, finite nucleon mass, thermal and plasma corrections are included in the proton to neutron conversion rates. The relic densities of ${}^4\text{He}$, D and ${}^7\text{Li}$ have been numerically obtained *via* a new updated version of the standard BBN code. In particular the theoretical uncertainty on ${}^4\text{He}$ is reduced to the order of 0.1 %.

PACS number(s): 98.80.Cq; 95.30.Cq; 11.10.Wx; 13.40.Ks

1 Introduction

Big Bang Nucleosynthesis (BBN) still represents one of the key subject of modern cosmology even if its clear understanding traces back to over 25 years ago [1]. The reason for this relies on the fact that BBN is one of the most powerful tools to study fundamental interactions, since light nuclei abundances are crucially depending on many elementary particle properties. As a well-known example, the ${}^4\text{He}$ abundance is strongly affected by the number of *effective* neutrino degrees of freedom, but others fascinating phenomena such as neutrino degeneracy or oscillation phenomena can be studied too, using the universe few seconds after the bang as a laboratory.

In the recent years, the experimental accuracy of the light primordial nuclei abundances, mainly the one of ${}^4\text{He}$, underwent a sort of revolution. The qualitative results of not too many years ago, suggesting that the ${}^4\text{He}$ mass fraction Y_4 was of the order of 0.25, recently turned in measurements with accuracies of the order of one percent. A similar good improvement has been obtained in both Deuterium (D) and ${}^7\text{Li}$ abundances $Y_2 \equiv D/H$ and $Y_7 \equiv {}^7\text{Li}/H$. In particular for D , measurements in distant Quasars Absorption line Systems (QAS) now represent a reliable estimate of the primordial value for Y_2 , which is only lowered by subsequent stellar processing. Paradoxically, the refinement of these experimental techniques, due to the uncertainties in the models describing stellar activity, is at the basis of large discrepancies between different set of results. Such discrepancies are possibly of systematic origin, or may reveal new aspects of cosmological evolution of the universe. The observations of Y_4 from regression to zero metallicity in blue compact galaxies in two independent surveys still produce two incompatible results, a *low* value [2],

$$Y_4^{(l)} = 0.234 \pm 0.002 \pm 0.005 \quad , \quad (1.1)$$

and a significantly higher one [3],

$$Y_4^{(h)} = 0.243 \pm 0.003 \quad . \quad (1.2)$$

A similar situation occurs in D measurements, where observations in different QAS, both at red shift larger than 3, give two results at bias for one order of magnitude [4, 5]

$$Y_2^{(l)} = (3.4 \pm 0.3) 10^{-5} \quad , \quad (1.3)$$

$$Y_2^{(h)} = (1.9 \pm 0.4) 10^{-4} \quad . \quad (1.4)$$

For the ${}^7\text{Li}$ abundance, the almost constant *Spite plateau* observed in the halo of POP II stars [6, 7]

$$Y_7^{(l)} = (1.6 \pm 0.36) 10^{-10} \quad , \quad (1.5)$$

is generally considered a reliable estimate of primordial abundance. Nevertheless, the observation of stars similar to the ones contributing to the Spite plateau, but with no traces of ${}^7\text{Li}$ [6, 8], seems to imply the presence of a depletion mechanism. A recent analysis based on a sample of 41 stars does not find any evidence of depletion mechanism or post-BBN creation and yields the primordial abundance [9]

$$Y_7^{(h)} = (1.73 \pm 0.21) 10^{-10} \quad . \quad (1.6)$$

A brief summary of the complete experimental situation on primordial abundances can be found in Ref. [10].

Probably, future measurements or a better understanding of the present data will clarify about the systematics. Nevertheless what is emerging from the above results is that the ${}^4\text{He}$ data are reaching a precision of the order of few percents. This fact requires a similar effort in the theoretical analysis, in order to reduce the uncertainty on the predictions at least at the same level of magnitude. In a previous paper [11] we performed a thoroughly analysis of all corrections to the proton/neutron conversion rates,

$$\begin{aligned} (a) \quad \nu_e + n &\rightarrow e^- + p \quad , & (d) \quad \bar{\nu}_e + p &\rightarrow e^+ + n \quad , \\ (b) \quad e^- + p &\rightarrow \nu_e + n \quad , & (e) \quad n &\rightarrow e^- + \bar{\nu}_e + p \quad , \\ (c) \quad e^+ + n &\rightarrow \bar{\nu}_e + p \quad , & (f) \quad e^- + \bar{\nu}_e + p &\rightarrow n \quad , \end{aligned} \quad (1.7)$$

which fix at the freeze out temperature $\sim 1 \text{ MeV}$ the neutron to proton density ratio. The Born rates, obtained in the tree level $V - A$ limit and with infinite nucleon mass, have been corrected to take into account basically three classes of relevant effects:

- i) electromagnetic radiative corrections, which largely contribute to the rates of the fundamental processes, in particular in the low temperature regime, $T \leq 0.1 \text{ MeV}$;

- ii) finite nucleon mass corrections, which are of the order of T/M_N or m_e/M_N , with m_e, M_N the electron and nucleon mass, respectively;
- iii) plasma effects, proportional to the surrounding plasma temperature, which both affect the microscopic process rates (a) – (f), as well as the neutrino to photon temperature ratio through e^\pm, γ equations of state.

The other main source of theoretical uncertainty comes from the partial knowledge of nuclear rates relevant for nuclei formation. Their numerical expressions, obtained by a convolution of the experimental data with a Boltzmann distribution, are affected by uncertainties of the order of 10% (see references quoted in [12]). More crucially, in many cases, these fits are known to well describe the data in a temperature interval which is only partially overlapping the one relevant for BBN, $0.01 \text{ MeV} \leq T \leq 10 \text{ MeV}$. However, both a Montecarlo analysis to sample the error distribution of the reaction cross sections [13], and a more recent method based on linear error propagation [14], show that, in particular for ${}^4\text{He}$ mass fraction, the effect is at most as large as the one due to the uncertainty on neutron lifetime τ_n , and smaller than 1%. Therefore it is theoretically justified to look, as in [11], for all sources of theoretical uncertainty up to this level of precision. The situation gets worse with D and ${}^7\text{Li}$, where the uncertainties due nuclear reactions can be as large as $(10 \div 30)\%$ [14].

This paper represents the natural companion to [11]. We have built a new updated version of the standard BBN code, which is available since many years [1, 12], where all corrections i)-iii) have been included. In particular we have also included the modified e^\pm, γ equations of state due to electromagnetic mass renormalization. In Section 2 we review the corrections to $n \leftrightarrow p$ Born rates, while in Section 4 we discuss the numerical method we have used to integrate the set of equations relevant for BBN, which are described in Section 3. The numerical results for light nuclei abundances, as functions of the final baryon to photon density ratio, η , the number of effective neutrino degrees of freedom, N_ν , and the neutron lifetime, τ_n , are reported in Section 5, where they are discussed and compared with the experimental data. We have also performed a fit of these abundances with a precision of the order of 0.1% in the interesting range for the parameters η, N_ν

and τ_n . Finally in Section 6 we give our conclusions.

2 Corrections to $n \leftrightarrow p$ Born rates

As is well known, the key parameter in determining the primordial ${}^4\text{He}$ mass fraction, Y_4 , is the value of the neutron to proton density ratio at the freeze-out temperature $T \sim 1 \text{ MeV}$, since almost all residual neutrons are captured in ${}^4\text{He}$ nuclei due to its large binding energy per nucleon. In order to make an accurate theoretical prediction for Y_4 it is necessary, though not sufficient, to have a reliable evaluation of the rates for the processes (1.7). An effort in this direction has been pursued in the last ten years by many authors. Recently, the entire set of corrections to the Born rates ω_B at the level of 1% accuracy have been recalculated in [11] and [15], with quite compatible results. In this Section we shortly summarize the main corrections $\Delta\omega/\omega_B$ coming from considering radiative, finite nucleon mass, and thermal effects. This short review is here included for the sake of completeness and to fix the notation. A detailed discussion of the subject can be found in our paper [11].

2.1 The Born rates

Let us consider as an example, the thermal averaged rate per nucleon for the neutron decay process (e). In the simple $V - A$ tree level, and in the limit of infinite nucleon mass, which we will refer to as *Born approximation*, one has

$$\omega_B(n \rightarrow e^- + \bar{\nu}_e + p) = \frac{G_F^2 (C_V^2 + 3C_A^2)}{2\pi^3} \int_0^\infty d|\mathbf{p}'| |\mathbf{p}'|^2 q_0^2 \Theta(q_0) [1 - F_\nu(q_0)] [1 - F_e(p'_0)], \quad (2.1)$$

where G_F is the Fermi coupling constant, C_V and C_A the nucleon vector and axial coupling. In our notation \mathbf{p}' and p'_0 are the electron momentum and energy, and q_0 the neutrino energy. The integration limits are imposed by the Θ -function, $q_0 \geq 0$. For reaction (e) we have $q_0 = M_n - M_p - p'_0 \equiv \Delta - p'_0$. The Fermi statistical distributions for e^\pm and neutrinos in the *comoving frame*, neglecting chemical potentials, are

$$F_e(p'_0) = [e^{\beta|p'_0|} + 1]^{-1}, \quad F_\nu(q_0) = [e^{\beta_\nu|q_0|} + 1]^{-1}, \quad (2.2)$$

with $\beta = 1/T$ and $\beta_\nu = 1/T_\nu$ ¹. All other rates for processes (a) – (d), (f) can be simply obtained from (2.1) properly changing the statistical factors and the expression for q_0 [11].

The accuracy of Born approximation can be tested by comparing, for example, the prediction for neutron lifetime with the experimental value $\tau_n^{ex} = (886.7 \pm 1.9) s$ [16]. Using $C_V = 0.9751 \pm 0.0006$ and $C_A/C_V = 1.2601 \pm 0.0025$ [16], Eq. (2.1) in the vanishing density limit gives $\tau_n \simeq 961 s$. Therefore, to recover the experimental value, a correction of about 8% is expected to come from radiative and/or finite nucleon mass effects. In the same way these corrections are also expected to contribute to all six processes (a)–(f) relevant for BBN. In addition to these, microscopic $n \leftrightarrow p$ reactions taking place in the early universe, also feel the presence of the surrounding plasma of γ and e^\pm pairs in thermodynamical equilibrium. Emission and absorption of real γ or e^\pm from the thermal bath can be taken into account using the finite temperature field theory in the real time formalism. This has been considered by several authors [17], and recently in [11].

2.2 Electromagnetic radiative corrections

It is customary to separate the electromagnetic radiative corrections to the Born amplitudes for processes (1.7) in *outer* and *inner* terms. The first ones involve the nucleon as a whole and consist in a multiplicative factor to the modulus squared of transition amplitude of the form

$$1 + \frac{\alpha}{2\pi} g(p'_0, q_0) \quad . \quad (2.3)$$

The function $g(p'_0, q_0)$ [18] depends on electron and neutrino energies and describes the deformation in the electron spectrum. Its effect on a freely decaying neutron is such to reduce the Born prediction for the lifetime of about 1.6%.

Inner corrections are sensible to nucleon structure details, and thus much more difficult to handle. They have been estimated in [19], studying corrections to the quark weak currents. Translating the quark-based description in the hadronic language, the inner corrections result in the additional multiplicative factor

$$1 + \frac{\alpha}{2\pi} \left(4 \ln \frac{M_Z}{M_p} + \ln \frac{M_p}{M_A} + 2C + A_g \right) \quad , \quad (2.4)$$

¹The ratio T_ν/T is fixed by entropy conservation and using the neutrino decoupling temperature [11] (see Section 2.4.1).

where the first term is the short-distance contribution and $A_g = -0.34$ is a perturbative QCD correction. The other two terms are related to the axial-induced contributions, with $M_A = (400 \div 1600)MeV$ a low energy cut-off in the short-distance part of the γW box diagram, and C related to the remaining long distance term.

The global effect of these two kind of corrections, improved by resumming all leading logarithmic corrections $\alpha^n \ln^n(M_Z)$ [20], is *via* the multiplicative factor

$$\mathcal{G}(p'_0, q_0) = \left[1 + \frac{\alpha}{2\pi} \left(\ln \frac{M_p}{M_A} + 2C \right) + \frac{\alpha(M_p)}{2\pi} [g(p'_0, q_0) + A_g] \right] S(M_p, M_Z) \quad , \quad (2.5)$$

where $\alpha(\mu)$ is the QED running coupling constant defined in the \overline{MS} scheme and $S(M_p, M_Z)$ a short distance rescaling factor, defined in [11].

Another effect to be considered, which can be in fact as large as few percents of the Born rates, is the so-called *Coulomb correction*, due to the rescattering of the electron in the field of the proton and leading to the Fermi function for Coulomb scattering

$$\mathcal{F}(p'_0) \simeq \left(1 + \alpha\pi \frac{p'_0}{|\mathbf{p}'|} \right) \quad . \quad (2.6)$$

However, this effect is only present when both electron and proton are in either the initial or final states, namely it only corrects the amplitudes of processes (a), (b), (e) and (f).

One may wonder if including the effects given by (2.5) and (2.6) the theoretical prediction for neutron decay is now compatible with the experimental results. Evaluating numerically the integral over the phase space one finds $\tau_n^{th} = 893.9$ s, still at variance with the experiment. Even adding all known sub-leading effects the agreement does not really improve [21]. As in Ref. [11] we take the point of view of rescaling all the rates (1.7), after including finite nucleon mass corrections (see next section), by the constant factor $1 + \delta_\tau = \tau_n^{th}/\tau_n^{ex} = 1.008$, which should be regarded as an energy independent correction to the weak process rates. This renormalization of the coupling guarantees the correct prediction for τ_n .

In Fig. 1 we report the Born rates ω_B for $n \leftrightarrow p$ processes, while in Fig. 2 we plot the corresponding radiative corrections, $\Delta\omega_R/\omega_B$. Their effect is particularly large, up to $\sim 8\%$, at low temperature.

2.3 Finite nucleon mass corrections

There are three additional contributions to the $n \leftrightarrow p$ rates which appear when one relaxes the approximation of infinitely massive nucleons. The leading effects are proportional to m_e/M_N or T/M_N , which, in the temperature range relevant for BBN, can be as large as the radiative corrections considered in the previous Section. This has been first pointed out in [22] and then also numerically evaluated in [11]. At order $1/M_N$ there are new couplings appearing in the expression of the weak hadronic current, the larger one coming from the weak magnetic moments of nucleons

$$J_\mu^{wm} = i \frac{G_F}{\sqrt{2}} \frac{f_2}{M_N} \bar{u}_p(p) \sigma_{\mu\nu} (p - q')^\nu u_n(q') \quad , \quad (2.7)$$

where, from CVC, $f_2 = V_{ud}(\mu_p - \mu_n)/2 = 1.81V_{ud}$. Both scalar and pseudoscalar contributions can be shown to be much smaller and negligible for the accuracy we are interested in. At the same order in inverse nucleon mass power it is also necessary to include the deformation of the allowed phase space for the relevant scattering and decay processes, due to nucleon recoiling. The sum of these two corrections for $n \leftrightarrow p$ rates with respect to the Born values, $\Delta\omega_M/\omega_B$, is plotted in Fig. 3.

The third effect is due to the initial nucleon thermal distribution. In the infinite nucleon mass limit, the average of weak rates over nucleon distribution is in fact trivial, since the nucleon is at rest in any frame. For finite M_N , by considering only $1/M_N$ terms, the effect of the thermal average over the thermal spreading of the nucleon velocity produces a purely *kinetic* correction $\Delta\omega_K$, whose expression can be reduced to a one dimensional integral over electron momentum which can be numerically evaluated. The explicit expression, which we do not report for brevity can be found in Section 4.2 and Appendix C of [11]. The ratios $\Delta\omega_K/\omega_B$ for $n \leftrightarrow p$ are reported in Fig. 4. Their size is rapidly growing with temperature, since they are proportional to the ratio T/M_N .

2.4 Thermal-Radiative corrections

The $n \leftrightarrow p$ rates, calculated as the processes would occur in vacuum, get slight corrections from the presence of the surrounding plasma of e^\pm pairs and γ . These are the so-called *thermal-radiative effects*.

To compute these corrections one may use the standard real time formalism for finite temperature field theory. According to this scheme, field propagators get additional contributions proportional to the number density of that particular specie in the surrounding medium. For γ and e^\pm we have

$$i \Delta_\gamma^{\mu\nu}(k) = - \left[\frac{i}{k^2} + 2\pi \frac{\delta(k^2)}{e^{\beta|k_0|} - 1} \right] g^{\mu\nu} = - \left[\frac{i}{k^2} + 2\pi \delta(k^2) B(k_0) \right] g^{\mu\nu} \quad , \quad (2.8)$$

$$i S_e(p') = \frac{i}{\not{p}' - m_e} - 2\pi \delta(p'^2 - m_e^2) F_e(p'_0) (\not{p}' + m_e) \quad . \quad (2.9)$$

The entire set of thermal corrections $\Delta\omega_{TR}$, at first order in its typical scale factor, i.e. $\alpha T/m_e$, have been computed by several authors [17] with quite different results. We have recently performed this lengthy calculation in [11], to which we refer for all details, and we have found a good agreement with the original result of first reference in [17], namely that they contribute to correct the Born rates only for less than 1%.

2.4.1 Radiative corrections on neutrino temperature

By assuming a sharp neutrino decoupling at $T_D = 2.3 \text{ MeV}$ [23], the ratio T_ν/T can be evaluated using entropy conservation [11]. This leads to the expression

$$\frac{T_\nu}{T} = \begin{cases} \left(\frac{\mathcal{I}(x_\gamma) + 2\mathcal{I}(x_e)}{\mathcal{I}(x_\gamma^D) + 2\mathcal{I}(x_e^D)} \right)^{1/3} & T \leq T_D \\ 1 & T > T_D \end{cases} \quad , \quad (2.10)$$

with

$$\mathcal{I}(x) = \int_0^\infty (y^2 + 2yx)^{1/2} (4y^2 + 8yx + 3x^2) [\exp(x+y) \pm 1]^{-1} dy \quad . \quad (2.11)$$

According to our notation $x_\alpha \equiv m_\alpha^R/T$ and $x_\alpha^D \equiv m_\alpha^R/T_D$ with $\alpha = \gamma, e$ (+ or - in the above integrand is for fermions or bosons, respectively). Note that m_γ^R and m_e^R are the effective masses that photons and e^\pm acquire in the heat bath due to their interactions with the background plasma (see Appendix A for details).

In [11] the neutrino temperature T_ν as a function of photon temperature T was evaluated by using in (2.10) the approximated expressions $m_\gamma^R \simeq 0$ and $m_e^R \simeq m_e + \alpha T^2/m_e$. This simplified expression for T_ν has been used in all previous sections in order to obtain the Born rates and their corrections as a function of T only. The difference between the neutrino temperature evaluated with the correct renormalized masses (A.1), (A.2), and

the one obtained with the simplified expressions results to be smaller than 0.01%. The corresponding effect on the rates (1.7) due to this small change in neutrino/photon temperature ratio, which can be seen as a further sub-leading thermal-radiative correction to Born rates, can be neglected at the level of precision we are interested in.

All thermal-radiative corrections to Born rates $\Delta\omega_{TR}/\omega_B$ are reported in Fig. 5. As evident from this plot, around the freeze-out temperature $T \sim 1 \text{ MeV}$, $\Delta\omega_{TR}$ only contribute as $\sim 0.4\%$ to the total rates. Thus they are clearly subdominant. Note that changing T_D in the range $(2 \div 3)\text{MeV}$ only affects T_ν/T for less than 0.2%.

2.5 The total rates for $n \leftrightarrow p$ reactions

In Fig. 6 we report the total corrections $\Delta\omega$ to Born rates ω_B . In order to use the corrected $n \leftrightarrow p$ rates $\omega = \omega_B + \Delta\omega$ in the BBN code, it is useful to fit their expressions as a function of the adimensional inverse photon temperature $z \equiv m_e/T$,

$$\omega(n \rightarrow p) = \frac{1}{\tau_n^{ex}} \exp(-q_{np} z) \sum_{l=0}^{13} a_l z^{-l} \quad , \quad 0.01 \text{ MeV} \leq T \leq 10 \text{ MeV} \quad (2.12)$$

$$\omega(p \rightarrow n) = \begin{cases} \frac{1}{\tau_n^{ex}} \exp(-q_{pn} z) \sum_{l=1}^{13} b_l z^{-l} & 0.1 \text{ MeV} \leq T \leq 10 \text{ MeV} \\ 0 & 0.01 \text{ MeV} \leq T < 0.1 \text{ MeV} \end{cases} \quad (2.13)$$

with

$$\begin{aligned} a_0 &= 1 & a_1 &= 0.160615 & a_2 &= 0.456817 \cdot 10^1 \\ a_3 &= -0.401109 \cdot 10^2 & a_4 &= 0.137254 \cdot 10^3 & a_5 &= -0.583644 \cdot 10^2 \\ a_6 &= 0.655938 \cdot 10^2 & a_7 &= -0.162185 \cdot 10^2 & a_8 &= 0.371109 \cdot 10^1 \\ a_9 &= -0.378497 & a_{10} &= 0.223840 \cdot 10^{-1} & a_{11} &= 0.723091 \cdot 10^{-5} \\ a_{12} &= -0.462476 \cdot 10^{-4} & a_{13} &= 0.186287 \cdot 10^{-5} & q_{np} &= 0.340994 \quad , \end{aligned} \quad (2.14)$$

$$\begin{aligned} b_1 &= 0.199695 \cdot 10^2 & b_2 &= -0.671993 \cdot 10^2 & b_3 &= 0.109230 \cdot 10^3 \\ b_4 &= -0.295891 \cdot 10^1 & b_5 &= 0.407831 \cdot 10^2 & b_6 &= -0.225830 \cdot 10^1 \\ b_7 &= 0.146751 & b_8 &= -0.185408 \cdot 10^{-2} & b_9 &= -0.205210 \cdot 10^{-3} \\ b_{10} &= 0.158424 \cdot 10^{-5} & b_{11} &= 0.369573 \cdot 10^{-6} & b_{12} &= -0.130731 \cdot 10^{-9} \\ b_{13} &= -0.329060 \cdot 10^{-9} & q_{pn} &= 2.89858 \quad . \end{aligned} \quad (2.15)$$

The fit has been obtained requiring that the fitting functions differ by less than 0.1% from the numerical values, while it is also a good approximation to consider a vanishing rate $\omega(p \rightarrow n)$ for $T \leq 0.1 \text{ MeV}$, see Eq. (2.13), since it is a rapidly decreasing function with $T \rightarrow 0$.

3 The set of equations for BBN

Let us consider N_{nuc} species of nuclides, whose number densities, $X_i = n_i/n_B$, are normalized with respect to the total baryon density n_B . The different nuclides are ordered in the following way: $n, H, D, {}^3H, {}^3He, {}^4He, {}^6Li, {}^7Li, {}^7Be, \dots$ (for the complete list see Ref. [12]). Denoting with $R(t)$ the universe scale factor, the BBN set of equations as functions of R, n_B, T, X_i , and of the electron chemical potential $\phi_e \equiv \mu_e/T$ reads²

$$\frac{\dot{R}}{R} = \sqrt{\frac{8\pi}{3M_P^2}} [\rho_\gamma + \rho_e + \rho_\nu + \rho_B]^{1/2} \quad , \quad (3.1)$$

$$\frac{\dot{n}_B}{n_B} = -3 \frac{\dot{R}}{R} = -\sqrt{\frac{24\pi}{M_P^2}} [\rho_\gamma + \rho_e + \rho_\nu + \rho_B]^{1/2} \quad , \quad (3.2)$$

$$L\left(\frac{m_e}{T}, \phi_e\right) = \frac{\pi^2 n_B}{2 T^3} \sum_j Z_j X_j \quad , \quad (3.3)$$

$$\begin{aligned} \dot{T} = & - \left\{ 3 \frac{\dot{R}}{R} [\rho_\gamma + p_\gamma + \rho_e + p_e + \Theta(T - T_D) (\rho_\nu + p_\nu) + p_B] \right. \\ & + \left. \frac{\partial \rho_e}{\partial \phi_e} \left(\sum_j \frac{\partial \phi_e}{\partial X_j} \dot{X}_j - 3 \frac{\dot{R}}{R} n_B \frac{\partial \phi_e}{\partial n_B} \right) + n_B \sum_j \left(\Delta M_j + \frac{3}{2} T \right) \dot{X}_j \right\} \\ & \times \left\{ \frac{d\rho_\gamma}{dT} + \frac{\partial \rho_e}{\partial T} + \frac{\partial \rho_e}{\partial \phi_e} \frac{\partial \phi_e}{\partial T} + \Theta(T - T_D) \frac{d\rho_\nu}{dT} + \frac{3}{2} n_B \sum_j X_j \right\}^{-1} \quad (3.4) \end{aligned}$$

$$\dot{X}_i = \sum_{j,k,l} N_i \left(\Gamma_{kl \rightarrow ij} \frac{X_l^{N_l} X_k^{N_k}}{N_l! N_k!} - \Gamma_{ij \rightarrow kl} \frac{X_i^{N_i} X_j^{N_j}}{N_i! N_j!} \right) \equiv \Gamma_i(X_j) \quad . \quad (3.5)$$

In the previous relations ρ and p denote the energy density and the pressure of an arbitrary particle specie. The function $L(z, y)$ in (3.3) is defined as

$$L(z, y) \equiv \frac{1}{2} \int_z^\infty dx x \sqrt{x^2 - z^2} \left(\frac{e^y}{e^x + e^y} - \frac{e^{-y}}{e^x + e^{-y}} \right) \quad , \quad (3.6)$$

$i, j, k, l = 1, \dots, N_{nuc}$, and the i -th nuclide, with charge and atomic number (Z_i, A_i) , has mass M_i and mass excess (M_u is the atomic mass unit)

$$\Delta M_i = M_i - A_i M_u \quad . \quad (3.7)$$

Moreover, in (3.5) we are considering in the sum a reaction between N_i nuclides of type i and N_j of type j which results in N_l nuclides of type l and N_k of type k , with its reverse

²We are using natural units $\hbar = c = k_B = 1$.

reaction. The energy density and the pressure of baryons take the form

$$\rho_B = n_B \left[M_u + \sum_j \left(\Delta M_j + \frac{3}{2} T \right) X_j \right] , \quad (3.8)$$

$$p_B = n_B T \sum_j X_j . \quad (3.9)$$

Eq. (3.1) is easily recognized as the Friedmann equation where we have neglected for simplicity the cosmological constant. Eq. (3.2) rules the scaling on n_B , whereas (3.3) states the neutrality of primordial plasma. From entropy conservation one gets (3.4), and (3.5) are the Boltzmann equations for the N_{nuc} nuclide number densities. Note that the presence of the Θ -function in (3.4) is connected with neutrino decoupling at $T = T_D$.³

In the set of equations (3.1)-(3.5) one can safely substitute Eq. (3.3) with an analogous relation, obtained expanding the l.h.s. of (3.3) with respect to ϕ_e ,

$$L(z, y) \simeq y \int_z^\infty dx x \sqrt{x^2 - z^2} \frac{e^x}{(e^x + 1)^2} \equiv y f^{-1}(z) . \quad (3.10)$$

In this case, Eq. (3.3) provides an explicit expression for $\phi_e = \phi_e(T, n_B, X_j)$,

$$\phi_e \simeq \frac{\pi^2}{2} f \left(\frac{m_e}{T} \right) \frac{n_B}{T^3} \sum_j Z_j X_j . \quad (3.11)$$

The consistency of this approach has been tested by means of an iterative check.

The set of equations (3.1)-(3.5) can be transformed in a set of $N_{nuc} + 1$ differential equations with the dimensionless variable $z = m_e/T$ as the evolution parameter. For numerical reasons, it is also better to turn the variable n_B into the dimensionless quantity $\hat{h} \equiv n_B/T^3$, which varies more slowly with z than n_B . In terms of these new variables the BBN set of equations becomes

$$\frac{d\hat{h}}{dz} = \left[1 - \widehat{H}(z, \hat{h}, X_j) G(z, \hat{h}, X_j) \right] \frac{3\hat{h}}{z} , \quad (3.12)$$

$$\frac{dX_i}{dz} = G(z, \hat{h}, X_j) \frac{\widehat{\Gamma}_i}{z} , \quad (3.13)$$

where the function G is

$$G(z, \hat{h}, X_j) = \left\{ \frac{\sum_\alpha (4\hat{\rho}_\alpha - z \frac{\partial \hat{\rho}_\alpha}{\partial z}) + 4\Theta(z_D - z)\hat{\rho}_\nu + \frac{3}{2}\hat{h} \sum_j X_j}{3 \left[\sum_\alpha (\hat{\rho}_\alpha + \hat{p}_\alpha) + \frac{4}{3}\Theta(z_D - z)\hat{\rho}_\nu + \hat{h} \sum_j X_j \right] \widehat{H} + \hat{h} \sum_j \left(z\Delta \widehat{M}_j + \frac{3}{2} \right) \widehat{\Gamma}_j} \right\} . \quad (3.14)$$

³We have assumed that all neutrinos decouple at the same temperature T_D . Actually muon and tau neutrinos decouple at a slightly larger temperature of 3.5 MeV , but nevertheless our approximation is largely consistent with the required precision on ${}^4\text{He}$ yields.

In the previous equations $z_D = m_e/T_D$, $\alpha = e, \gamma$, and we have considered the dimensionless Hubble parameter $\widehat{H} = H/m_e$,

$$\widehat{H}(z, \hat{h}, X_j) = \sqrt{\frac{8\pi}{3}} \frac{m_e}{M_P} \frac{1}{z^2} \left[\hat{\rho}_\gamma + \hat{\rho}_e + \hat{\rho}_\nu + \hat{h} \left(z\widehat{M}_u + \sum_j \left(z\Delta\widehat{M}_j + \frac{3}{2} \right) X_j \right) \right]^{1/2}, \quad (3.15)$$

and the quantities $\widehat{M}_u = M_u/m_e$, $\Delta\widehat{M}_j = \Delta M_j/m_e$, $\widehat{\Gamma}_j = \Gamma_j/m_e$. Energy densities and pressures have been adimensionalized dividing by T^4 . In Eq.s (3.12) and (3.13) we have neglected the terms containing the derivatives of chemical potential. In Appendix A we report the expressions for \hat{p}_α and $\hat{\rho}_\alpha$ evaluated taking into account the γ and e^\pm electromagnetic mass renormalization. As already mentioned in the previous section this effect, changing the γ and e^\pm equations of state, slightly modifies the T_ν/T ratio too. In order to speed up the numerical computation a fit of \hat{p}_α and $\hat{\rho}_\alpha$ as functions of z has been performed and is also reported in Appendix A.

The initial value for (3.12) is provided in terms of the final baryon to photon density ratio η according to the equation

$$\hat{h}_{in} = \frac{2\zeta(3)}{\pi^2} \eta_{in} = \frac{11}{4} \frac{2\zeta(3)}{\pi^2} \eta. \quad (3.16)$$

The condition of Nuclear Statistical Equilibrium (NSE), which is satisfied with high accuracy at the initial temperature $T_{in} = 10 \text{ MeV}$, is then fixing the initial nuclide relative abundances. From NSE one gets, for an arbitrary i -th nuclide with g_i internal degrees of freedom,

$$X_i(T_{in}) = \frac{g_i}{2} \left(\zeta(3) \sqrt{\frac{8}{\pi}} \right)^{A_i-1} A_i^{\frac{3}{2}} \left(\frac{T_{in}}{M_N} \right)^{\frac{3}{2}(A_i-1)} \eta^{A_i-1} X_p^{Z_i} X_n^{A_i-Z_i} \exp \left\{ \frac{B_i}{T_{in}} \right\}, \quad (3.17)$$

where B_i denotes the binding energy.

4 Numerical Method

The most critical part of the BBN code concerns the method of numerical resolution of the set of differential equations (3.12), (3.13). In fact, since at high temperatures nuclear reactions proceed in both forward and reverse directions with almost equal rapidity, the r.h.s. of (3.13) results to be a small difference of large numbers. When this occurs the

Table 1

1)	$n \leftrightarrow p$
2)	$T \leftrightarrow {}^3\text{He}$
3)	$p + n \leftrightarrow D + \gamma$
4)	$n + D \leftrightarrow T + \gamma$
5)	$n + {}^3\text{He} \leftrightarrow {}^4\text{He} + \gamma$
6)	$n + {}^6\text{Li} \leftrightarrow {}^7\text{Li} + \gamma$
7)	$n + {}^3\text{He} \leftrightarrow T + p$
8)	$n + {}^7\text{Be} \leftrightarrow {}^7\text{Li} + p$
9)	$n + {}^6\text{Li} \leftrightarrow {}^4\text{He} + T$
10)	$n + {}^7\text{Be} \leftrightarrow {}^4\text{He} + {}^4\text{He}$
11)	$p + D \leftrightarrow {}^3\text{He} + \gamma$
12)	$p + T \leftrightarrow {}^4\text{He} + \gamma$
13)	$p + {}^6\text{Li} \leftrightarrow {}^7\text{Be} + \gamma$
14)	$p + {}^6\text{Li} \leftrightarrow {}^4\text{He} + {}^3\text{He}$
15)	$p + {}^7\text{Li} \leftrightarrow {}^4\text{He} + {}^4\text{He}$
16)	$D + {}^4\text{He} \leftrightarrow {}^6\text{Li} + \gamma$
17)	$T + {}^4\text{He} \leftrightarrow {}^7\text{Li} + \gamma$
18)	${}^3\text{He} + {}^4\text{He} \leftrightarrow {}^7\text{Be} + \gamma$
19)	$D + D \leftrightarrow {}^3\text{He} + n$
20)	$D + D \leftrightarrow T + p$
21)	$D + T \leftrightarrow {}^4\text{He} + n$
22)	$D + {}^3\text{He} \leftrightarrow {}^4\text{He} + p$
23)	${}^3\text{He} + {}^3\text{He} \leftrightarrow {}^4\text{He} + p + p$
24)	$D + {}^7\text{Li} \leftrightarrow {}^4\text{He} + {}^4\text{He} + n$
25)	$D + {}^7\text{Be} \leftrightarrow {}^4\text{He} + {}^4\text{He} + p$

Table 1: The reduced network of nuclear reactions.

numerical problem is said *stiff*. As a consequence, the step size is limited more severely by the requirement of stability than by the accuracy of the numerical technique. In other words, to preserve integration stability it is required to use a shorter step size than what would be dictated by accuracy only. In order to manage the problem, we use a NAG routine implementing a method belonging to the class of Backward Differentiation Formulas (BDFs) [24]. This is quite a new approach for BBN codes. In fact the standard code [1, 12] uses instead the implicit differentiating method (backward Euler scheme) [24] for writing the r.h.s. of (3.13) and a Runge-Kutta solver.

Few comments on the different numerical methods are in order. Let us consider the

differential equation

$$\frac{dy(t)}{dt} = f(t, y(t)) \quad . \quad (4.1)$$

In the Runge-Kutta methods the solution at t_{i+1} is completely determined by its value at t_i (one-step methods), namely the solver has *no memory*. A different approach is provided by a wide class of numerical methods referred to as *multistep methods* like BDFs. Here, the values of the solution at t_k ($k = i, i - 1, \dots, i - p$), $y(t_k) \equiv y_k$, previously computed, and the unknown value $y(t_{i+1}) \equiv y_{i+1}$, are interpolated by a polynomial, $P(t; y_{i+1}, y_i, \dots)$, in order to approximate the solution and its derivative. Substituting in the differential equation,

$$\frac{dP}{dt}(t_{i+1}; y_{i+1}, y_i, \dots) \simeq f(t_{i+1}, y_{i+1}) \quad , \quad (4.2)$$

one obtains a family of BDFs,

$$\begin{aligned} (t_{i+1} - t_i) f(t_{i+1}, y_{i+1}) &\simeq P(t_{i+1}; y_{i+1}, y_i, \dots) - P(t_i; y_{i+1}, y_i, \dots) \\ &= \alpha_0 y_{i+1} + \alpha_1 y_i + \dots \quad . \end{aligned} \quad (4.3)$$

Two methods can be used for solving the previous equation in the implicit case, $\alpha_0 \neq 0$: functional iteration and Newton's method. In the former case some initial guess is taken for y_{i+1} and refined by iteration. In the latter case, one linearizes Eq. (4.3) by expanding f around y_i . The new point, y_{i+1} , is then found by inverting a matrix, in a way similar to the backward Euler scheme. The NAG routine implements both methods and incorporates an error control test, which drives the step-size adjustment.

The nuclear reaction network used in the code includes all the 88 reactions between the 26 nuclides present in the standard code [1, 12]. We used the same nuclear rate data of the standard code, which are collected and updated in [25]. In order to reduce the computation time one can also choose a reduced network, made of the 25 reactions between 9 nuclides listed in Table 1. Using the complete network we have verified that the reduced one affects the abundances for no more than 0.01 %, while it greatly reduces the evaluation time.

5 Results on Light Element Abundances

The reliable numerical code just discussed can now be used to study the effect of the different corrections to $n \leftrightarrow p$ Born rates on light elements abundances. By definition

$$Y_2 = \frac{X_3}{X_2} \quad , \quad Y_3 = \frac{X_5}{X_2} \quad , \quad Y_4 = \frac{M_6 X_6}{\sum_j M_j X_j} \quad , \quad Y_7 = \frac{X_8}{X_2} \quad . \quad (5.1)$$

In the first two rows of Table 2 are shown the predictions for Y_2 , Y_3 , Y_4 and Y_7 at $\eta = 5 \cdot 10^{-10}$, corresponding to the complete $n \leftrightarrow p$ rates, ω_{Tot} , and to the Born approximation, ω_B ⁴. As it is clear from Table 2, the main effect of the corrections, which results into the enhancement of the $n \rightarrow p$ conversion rate, is to allow a smaller number of neutrons to survive till the onset of nucleosynthesis. This ends up in a smaller fraction of elements which fix neutrons with respect to hydrogen.

The effects on light element yields due to the various corrections with respect to the Born predictions are also reported in Table 2. For all nuclides the pure radiative correction $\Delta\omega_R$ provides the dominant contribution, while the finite nucleon mass effects, the kinetic and the thermal-radiative ones almost cancel each other. Finally the last row reports the further contribution due to the additional term required to recover the experimental neutron lifetime [11].

If we make use of the results of [14] to quantify the uncertainties coming from nuclear reaction processes, we observe that only for Y_4 the radiative correction affects the Born result by an amount larger than the theoretical uncertainties, including nuclear reactions. For 4He mass fraction in fact, the theoretical uncertainty due to nuclear reaction rates is estimated to be of the order of 0.1% and thus comparable with the uncertainty due to the experimental error on neutron lifetime. For D , 3He and 7Li the uncertainty due to the poor knowledge of nuclear reaction rates is estimated to be of the order of (10 ÷ 30)% [14], thus completely covering any radiative/thermal correction on $n \leftrightarrow p$ rates.

In Fig. 7 the predictions on Y_4 are shown versus η for $N_\nu = 2, 3, 4$ and for a 1 σ variation of τ_n^{ex} . The two experimental estimates for the primordial 4He mass fraction, $Y_4^{(l)}$ and $Y_4^{(h)}$, as horizontal bands, are also reported. Figs 8 and 9 show the predictions

⁴Note that, according to our notation, with ω_B we denote the pure Born predictions for $n \leftrightarrow p$ rates without any constant rescaling of coupling to account for the experimental value of neutron lifetime (see Section 2.2).

Table 2

	Y_2	Y_3	Y_4	Y_7
ω_{Tot}	$0.3638 \cdot 10^{-4}$	$0.1175 \cdot 10^{-4}$	0.2446	$0.2814 \cdot 10^{-9}$
ω_B	$0.3727 \cdot 10^{-4}$	$0.1184 \cdot 10^{-4}$	0.2550	$0.2873 \cdot 10^{-9}$
$\Delta\omega_R$	-2.3%	-2.8%	-3.8%	-1.9%
$\Delta\omega_M$.2%	.1%	.3%	.2%
$\Delta\omega_K$.2%	.1%	.3%	.2%
$\Delta\omega_{TR}$	-.6%	-.1%	-.7%	-.4%
$\delta_\tau\omega_T$	-.3%	-.1%	-.6%	-.3%

Table 2: The predictions on light element abundances obtained with the numerical code for $\eta = 5 \cdot 10^{-10}$ and $N_\nu = 3$. In the lower rows the effect of the various corrections is reported.

for D and 7Li abundances. Note that, due to the negligible variation of Y_2 and Y_7 on small τ_n changes, no splitting of predictions for 1σ variation of τ_n^{ex} is present.

A fit, up to 1% accuracy, of the relevant observables Y_2 , Y_3 , Y_4 and Y_7 as a function of $x = \log_{10}(10^{10}\eta)$, N_ν and τ_n has been performed. The following expressions have been obtained

$$10^3 \cdot Y_2 = \left[\sum_{i=0}^4 a_i x^i + a_5 (N_\nu - 3) \right] \exp \{ a_6 x + a_7 x^2 \} \quad , \quad (5.2)$$

$$10^5 \cdot Y_3 = \left[\sum_{i=0}^4 a_i x^i + a_5 (N_\nu - 3) \right] \exp \{ a_6 x \} \quad , \quad (5.3)$$

$$10 \cdot Y_4 = \sum_{i=0}^5 a_i x^i + a_6 (\tau - \tau_{ex}) + a_7 (N_\nu - 3) + a_8 x (\tau - \tau_{ex}) + a_9 x (N_\nu - 3) \quad (5.4)$$

$$10^9 \cdot Y_7 = \left[\sum_{i=0}^3 a_i x^i + a_4 (N_\nu - 3) + a_5 x (N_\nu - 3) \right] \exp \left\{ \sum_{i=1}^4 a_{5+i} x^i \right\} \quad , \quad (5.5)$$

where $\tau_{ex} = 886.7 s$ and the values of the fit coefficients are reported in Table 3.

Neutrino decoupling has been shown by many authors [26] to be a process which still

Table 3

Coeff.	$10^3 \cdot Y_2$	$10^5 \cdot Y_3$	$10 \cdot Y_4$	$10^9 \cdot Y_7$
a_0	0.4854	3.325	2.209	0.5419
a_1	0.2919	0.1496	0.5548	-0.5981
a_2	-0.3516	1.597	-0.6491	-1.914
a_3	0.5048	-1.923	0.7661	4.521
a_4	-0.4269	1.312	-0.5366	0.1587
a_5	$0.7772 \cdot 10^{-1}$	0.1782	0.1614	-0.3256
a_6	-4.397	-1.705	$0.2059 \cdot 10^{-2}$	-4.102
a_7	0.5925	/	0.1300	5.072
a_8	/	/	$-0.4156 \cdot 10^{-4}$	-1.209
a_9	/	/	$0.7433 \cdot 10^{-2}$	-0.6269

Table 3: Values of the fit coefficients (5.2)-(5.5) for light element abundances.

takes place when e^\pm pairs annihilate. This implies that neutrinos are in fact slightly reheated during this annihilation process and their final distribution in momentum space shows an interesting non equilibrium shape. In Ref. [27] it is estimated that the effect on Y_4 due to the inclusion of this slight neutrino heating is very small, $\delta Y_4 \sim 1.5 \cdot 10^{-4}$, in the whole range $10^{-10} \leq \eta \leq 10^{-9}$. We have included this constant correction to Y_4 prediction.

From the fit reported in Eq. (5.4) it is easy to quantify the theoretical error on Y_4 . Since this is basically due to the uncertainty on τ_n we have

$$\frac{\Delta Y_4}{Y_4} = \frac{(a_6 + a_8 x) \Delta \tau_n}{10 Y_4} \leq 0.1\% \quad . \quad (5.6)$$

In Fig. 10, our prediction for Y_4 of Eq. (5.4) with $N_\nu = 3$ and $\tau_n = 885.3$ s, is compared with an analogous fit, Y'_4 , performed in [10]. The agreement between the two expressions

obtained by independent codes is up to 1% in the relevant range for η .

In Fig. 11 we present the results of a likelihood analysis of the theoretical predictions obtained with the numerical code for the four combinations of experimental results: a) high D , low 4He ; b) high D , high 4He ; c) low D , low 4He ; d) low D , high 4He , and using the low value for 7Li abundance. In particular, we plot the product of gaussian distribution for D , 4He and 7Li centered around the measured values and with their corresponding experimental errors,

$$\begin{aligned}
 L(N_\nu, x) &= \exp \left\{ \frac{-(Y_2(N_\nu, x) - Y_2^{ex})^2}{2\sigma_2^2} \right\} \exp \left\{ \frac{-(Y_4(N_\nu, x) - Y_4^{ex})^2}{2\sigma_4^2} \right\} \\
 &\times \exp \left\{ \frac{-(Y_7(N_\nu, x) - Y_7^{ex})^2}{2\sigma_7^2} \right\} .
 \end{aligned} \tag{5.7}$$

Notice that all functions have been normalized to unity in the maximum. As is clear from the plots, the analysis prefers the high value of D (plots a) and b)). In both cases the distributions are centered in the range $x \in 0.2 \div 0.4$, but at $N_\nu \sim 3$ for low 4He and $N_\nu \sim 3.5$ for high 4He . For low D the compatibility with experimental data is worse. Note that c) and d) distributions have been multiplied by a factor of 25 and 100 respectively and centered in the range $x \in 0.6 \div 0.8$, and at $N_\nu \sim 2$ for low 4He and $N_\nu \sim 3$ for high 4He . The better agreement at 1σ of the data set a) and b) with the theoretical predictions is basically due to the effect of 7Li data which corresponds to values for η compatible with low D data of c) and d) at 2σ only. It should be mentioned however that these results only take into account experimental errors, so that the confidence level regions in the $N_\nu - x$ plane would be broader by convoluting the considered distributions with the ones containing the theoretical error.

6 Conclusions

In this paper a detailed study of the effects on light element yields of the radiative, finite nucleon mass, thermal and plasma corrections to Born rates (1.7) has been carried out. The aim of such an analysis was to reduce the error on, basically, Y_4 to less than 1%, which is motivated by the most recent experimental determinations for 4He abundance. This accurate analysis has been performed using an update version of the BBN standard code [1, 12]. A different numerical approach, based on BDF techniques has been implemented

to solve the stiff Boltzmann equations for nuclei densities. The numerical results for ${}^4\text{He}$ mass fraction almost confirm the computation reported in Ref. [10], while the theoretical error, also including the propagation of uncertainties on nuclear processes, as estimated in [14], is of the order of 0.1%. Our analysis shows that the preferred experimental values are high value for D and low one for ${}^4\text{He}$, in which case the distribution is centered at $x \sim 0.3$ and $N_\nu \sim 3$.

A Radiative corrections to e^\pm , γ equations of state

In an accurate description of the primordial plasma it is important to consider the electromagnetic correction to the e^\pm and γ equations of state induced by the e^\pm and γ mass renormalization.

As well known, the photon renormalized mass, up to first order correction in the electromagnetic coupling constant α , reads [28]

$$m_\gamma^R(z) \simeq m_e \frac{2}{z} \sqrt{\frac{\alpha}{\pi}} \left[\int_z^\infty dx \frac{\sqrt{x^2 - z^2}}{1 + e^x} \right]^{1/2}, \quad (\text{A.1})$$

and for e^\pm [17]

$$m_e^R(z, y) \simeq m_e \left\{ 1 + \frac{\alpha}{\pi z^2} \left[\frac{\pi^2}{3} + \int_z^\infty \left(2\sqrt{x^2 - z^2} + \frac{z^2}{2\sqrt{y^2 - z^2}} \log \Lambda \right) \frac{dx}{1 + e^x} \right] \right\}, \quad (\text{A.2})$$

where $z \equiv m_e/T$, $y \equiv E_e/T$ and

$$\Lambda(x, y, z) = \frac{x^2 y^2 - \left(z^2 + \sqrt{x^2 - z^2} \sqrt{y^2 - z^2} \right)^2}{x^2 y^2 - \left(z^2 - \sqrt{x^2 - z^2} \sqrt{y^2 - z^2} \right)^2}. \quad (\text{A.3})$$

Note that in Eq.s (A.1) and (A.2) one can neglect the contribution of electron chemical potential, $\phi_e \equiv \mu_e/T$, due to its small value.

By using (A.1) and (A.2) in the expressions of ρ_γ , p_γ , ρ_e , p_e one gets the latter quantities as functions of z only. Since the e^\pm and γ energy densities and pressures have to be used in a BBN code, in order to speed up the computation one can fit these quantities as function of z and use these fits in the evolution equations. The fitted expressions for the dimensionless electron energy density and pressure, $\hat{\rho}_e = \rho_e/T^4$ and $\hat{p}_e = p/T^4$, in the range $z \in [0.05, 8.52]$ ($\hat{\rho}_e = \hat{p}_e = 0$ for $z > 8.52$), result to be

$$\begin{aligned} \hat{\rho}_e(z) &= 1.145 + 0.33981 \cdot 10^{-1} z - 0.14543 z^2 + 0.25507 \cdot 10^{-1} z^3 - 0.54168 \cdot 10^{-3} z^4 \\ &- 0.11263 \cdot 10^{-3} z^5 - 0.29742 \cdot 10^{-5} z^6 + 0.38331 \cdot 10^{-6} z^7 + 0.45263 \cdot 10^{-7} z^8 \\ &+ 0.19241 \cdot 10^{-8} z^9 - 0.96597 \cdot 10^{-10} z^{10} - 0.19505 \cdot 10^{-10} z^{11} - 0.14079 \cdot 10^{-12} z^{12}, \end{aligned} \quad (\text{A.4})$$

$$\begin{aligned} \hat{p}_e(z) &= \left(0.3786 + 0.19126 \cdot 10^{-1} z - 0.63895 \cdot 10^{-1} z^2 + 0.32085 \cdot 10^{-1} z^3 - 0.48501 \cdot 10^{-2} z^4 \right. \\ &- 0.16611 \cdot 10^{-3} z^5 + 0.82922 \cdot 10^{-4} z^6 + 0.79884 \cdot 10^{-5} z^7 - 0.60619 \cdot 10^{-6} z^8 \end{aligned}$$

$$- 0.19568 \cdot 10^{-6} z^9 - 0.10921 \cdot 10^{-7} z^{10} + 0.38564 \cdot 10^{-8} z^{11}) e^{-0.13145 z^2} . \quad (\text{A.5})$$

Moreover, in the considered temperature range, one can show that $\hat{\rho}_\gamma = \rho_\gamma/T^4$ only varies between 0.6580 and 0.6573, and $\hat{p}_\gamma = p_\gamma/T^4$ between 0.2193 and 0.2187. Thus, for simplicity, one can assume $\hat{\rho}_\gamma$ constant and equal to the average value 0.6577, and to 0.2190 for \hat{p}_γ .

References

- [1] R.V. Wagoner, W.A. Fowler, and F. Hoyle, *Astrophys. J.* **148** (1967) 3;
R.V. Wagoner, *Astrophys. J. Suppl.* **18** (1969) 247; R.V. Wagoner, *Astrophys. J.* **179** (1973) 343.
- [2] B.E.J. Pagel, E.A. Simonson, R.J. Terlevich, and M. Edmunds, *MNRAS* **255** (1992) 325;
E. Skillman and R.C. Kennicutt, *Astrophys. J.* **411** (1993) 655;
E. Skillman, R.J. Terlevich, R.C. Kennicutt, D.R. Garnett, and E. Terlevich, *Astrophys. J.* **431** (1994) 172.
- [3] Y.I. Izotov, T.X. Thuan, and V.A. Lipovetsky, *Astrophys. J.* **435** (1994) 647; *Ap.J.S.* **108** (1997) 1.
- [4] R.F. Carswell, M. Rauch, R.J. Weymann, A.J. Cooke, and J.K. Webb, *MNRAS* **268** (1994) L1;
A. Songaila, L.L. Cowie, C. Hogan, and M. Rugers, *Nature* **368** (1994) 599;
M. Rugers and C.J. Hogan, *A.J.* **111** (1996) 2135;
R.F. Carswell, *et al.* *MNRAS* **278** (1996) 518;
E.J. Wampler, *et al.*, *A.A.* **316** (1996) 33;
J.K. Webb, R.F. Carswell, K.M. Lanzetta, R. Ferlet, M. Lemoine, A. Vidal-Madjar, and D.V. Bowen, *Nature* **388** (1997) 250;
D. Tytler *et al.*, astro-ph/9810217 (1998).

- [5] D. Tytler, X.-M. Fan, and S. Burles, *Nature* **381** (1996) 207;
S. Burles and D. Tytler, *Astrophys. J.* **460** (1996) 584.
- [6] J.A. Thorburn, *Astrophys. J.* **421** (1994) 318.
- [7] P. Molaro, F. Primas, and P. Bonifacio, *Astron. Astrophys.* **295** (1995) L47.
- [8] S.G. Ryan, J.E. Norris, and T.C. Beers, *Astrophys. J.* **506** (1998) 892.
- [9] P. Bonifacio and P. Molaro, *Mon. Not. Roy. Astron. Soc.* **285** (1997) 847.
- [10] S. Sarkar, astro-ph/9903183.
- [11] S. Esposito, G. Mangano, G. Miele, and O. Pisanti, *Nucl. Phys.* **B540** (1999) 3.
- [12] L. Kawano, preprint FERMILAB-Pub-88/34-A; preprint FERMILAB-Pub-92/04-A.
- [13] L.M. Krauss and P. Romanelli, *Astrophys. J.* **358** (1990) 47;
P.J. Kernan and L.M. Krauss, *Phys. Rev. Lett.* **72** (1994) 3309.
- [14] G. Fiorentini, E. Lisi, S. Sarkar, and F.L. Villante, *Phys. Rev.* **D58** (1998) 063506.
- [15] R.E. Lopez and M.S. Turner, *Phys. Rev.* **D59** (1999) 103502.
- [16] C. Caso *et al.*, *Eur. Phys. Jour.* **C3** (1998) 1.
- [17] D.A. Dicus, E.W. Kolb, A.M. Gleeson, E.C.G. Sudarshan, V.L. Teplitz, and M.S. Turner, *Phys. Rev.* **D26** (1982) 2694;
J.L. Cambier, J.R. Primack, and M. Sher, *Nucl. Phys.* **B209** (1982) 372;
J.F. Donoghue, B.R. Holstein, and R.W. Robinett, *Ann. Phys. (N.Y.)* **164** (1985) 23;
J.F. Donoghue and B.R. Holstein, *Phys. Rev.* **D28** (1983) 340 and *Phys. Rev.* **D29** (1984) 3004;
A.E. Johansson, G. Peresutti, and B.S. Skagerstam, *Nucl. Phys.* **B278** (1986) 324;
W. Keil, *Phys. Rev.* **D40** (1989) 1176;
R. Baier, E. Pilon, B. Pire, and D. Schiff, *Nucl. Phys.* **B 336** (1990) 157;
W. Keil and R. Kobes, *Physica A* **158** (1989) 47;
M. LeBellac and D. Poizat, *Z. Phys.* **C47** (1990) 125;

- T. Altherr and P.Aurenche, *Phys. Rev.* **D40** (1989) 4171;
R.L. Kobes and G.W. Semeneff, *Nucl. Phys.* **B260** (1985) 714 and **B272** (1986) 329;
R.F. Sawyer, *Phys. Rev.* **D53** (1996) 4232;
I.A. Chapman, *Phys. Rev.* **D55** (1997) 6287;
S. Esposito, G. Mangano, G. Miele, and O. Pisanti, *Phys. Rev.* **D58** (1998) 105023.
- [18] A. Sirlin, *Phys. Rev.* **164** (1967) 1767.
- [19] W.J. Marciano and A. Sirlin, *Phys. Rev. Lett.* **56** (1986) 22.
- [20] W.J. Marciano and A. Sirlin, *Phys. Rev. Lett.* **46** (1981) 163.
- [21] D.M. Wilkinson, *Nucl. Phys.* **A377** (1982) 474.
- [22] D. Seckel, preprint BA-93-16, hep-ph/9305311;
R. E. Lopez, M. S. Turner, and G. Gyuk, *Phys. Rev.* **D56** (1997) 3191.
- [23] K. Enqvist, K. Kainulainen, and V. Semikoz, *Nucl. Phys.* **B374** (1992) 392.
- [24] B.P. Flannery, W.H. Press, S.A. Teukolsky, and W.T. Vetterling, *Numerical Recipes in Fortran*, Cambridge University Press.
- [25] For the expressions of the rates see the Web sites:
<http://www.phy.ornl.gov/astrophysics/data/data.html> or
http://pntpm.ulb.ac.be/Nacre/barre_database.htm.
- [26] M.A. Herrera and S. Hacyan, *Ap. J.* **336** (1989) 539;
N.C. Rana and B. Mitra, *Phys. Rev.* **D44** (1991) 393;
S. Dodelson and M.S. Turner, *Phys. Rev.* **D46** (1992) 3372;
A.D. Dolgov and M. Fukugita, *Phys. Rev.* **D46** (1992) 5378;
N.Y. Guedin and O.Y. Guedin, astro-ph/9712199;
S. Hannestad and J. Madsen, *Phys. Rev.* **D52** (1995) 1764;
A.D. Dolgov, S.H. Hansen, and D.V. Semikoz, *Nucl. Phys.* **B503** (1997) 426.
- [27] B. Fields, S. Dodelson, and M.S. Turner, *Phys. Rev.* **D47** (1993) 4309.
- [28] K. Ahmed and S.S. Masood, *Annals Phys.* **207** (1991) 460.

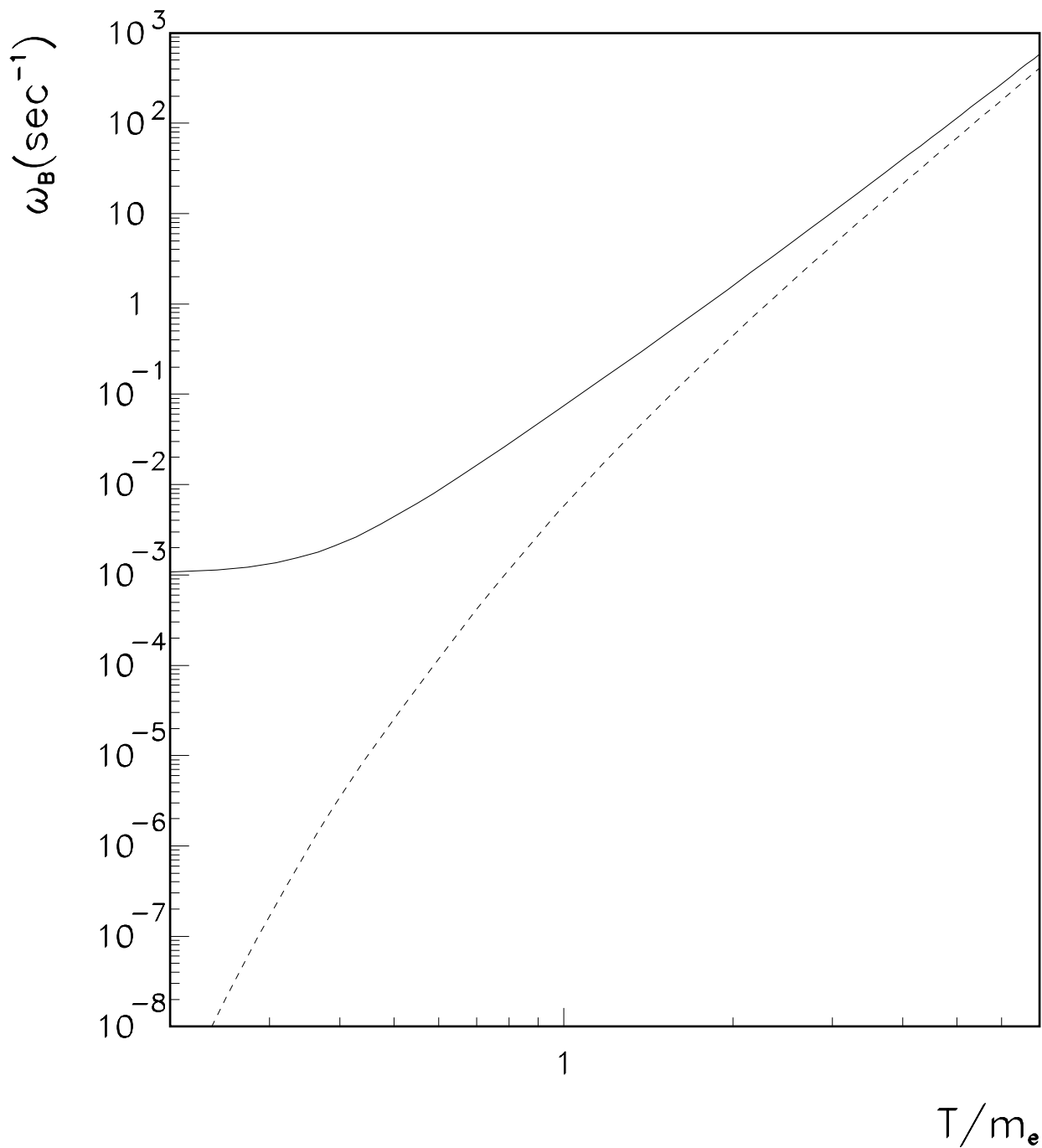


Figure 1: The total Born rates, ω_B , for $n \rightarrow p$ (solid line) and $p \rightarrow n$ transitions (dashed line). This notation is adopted hereafter.

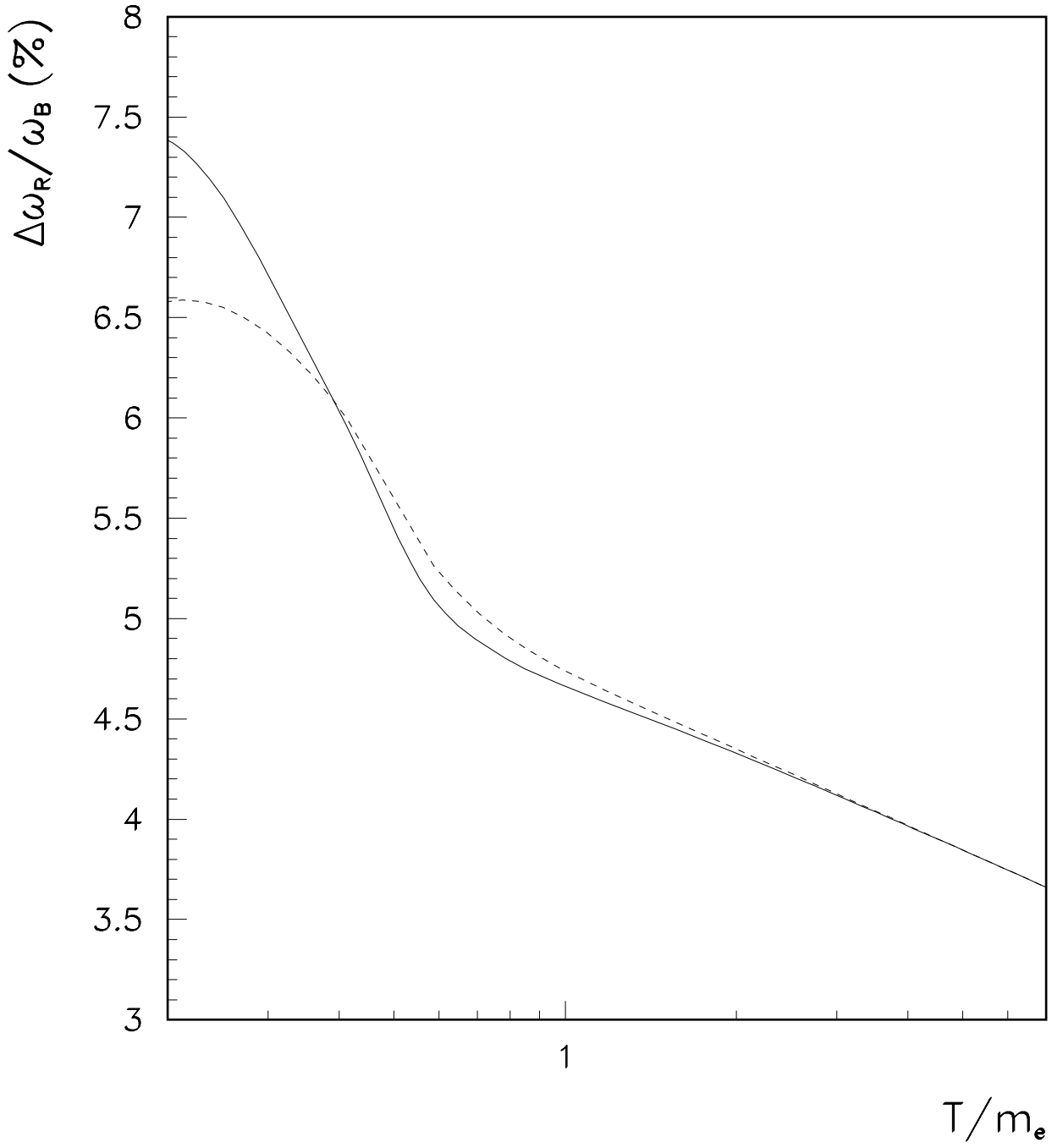


Figure 2: The radiative corrections to Born rates, $\Delta\omega_R/\omega_B$, for $n \leftrightarrow p$ transitions.

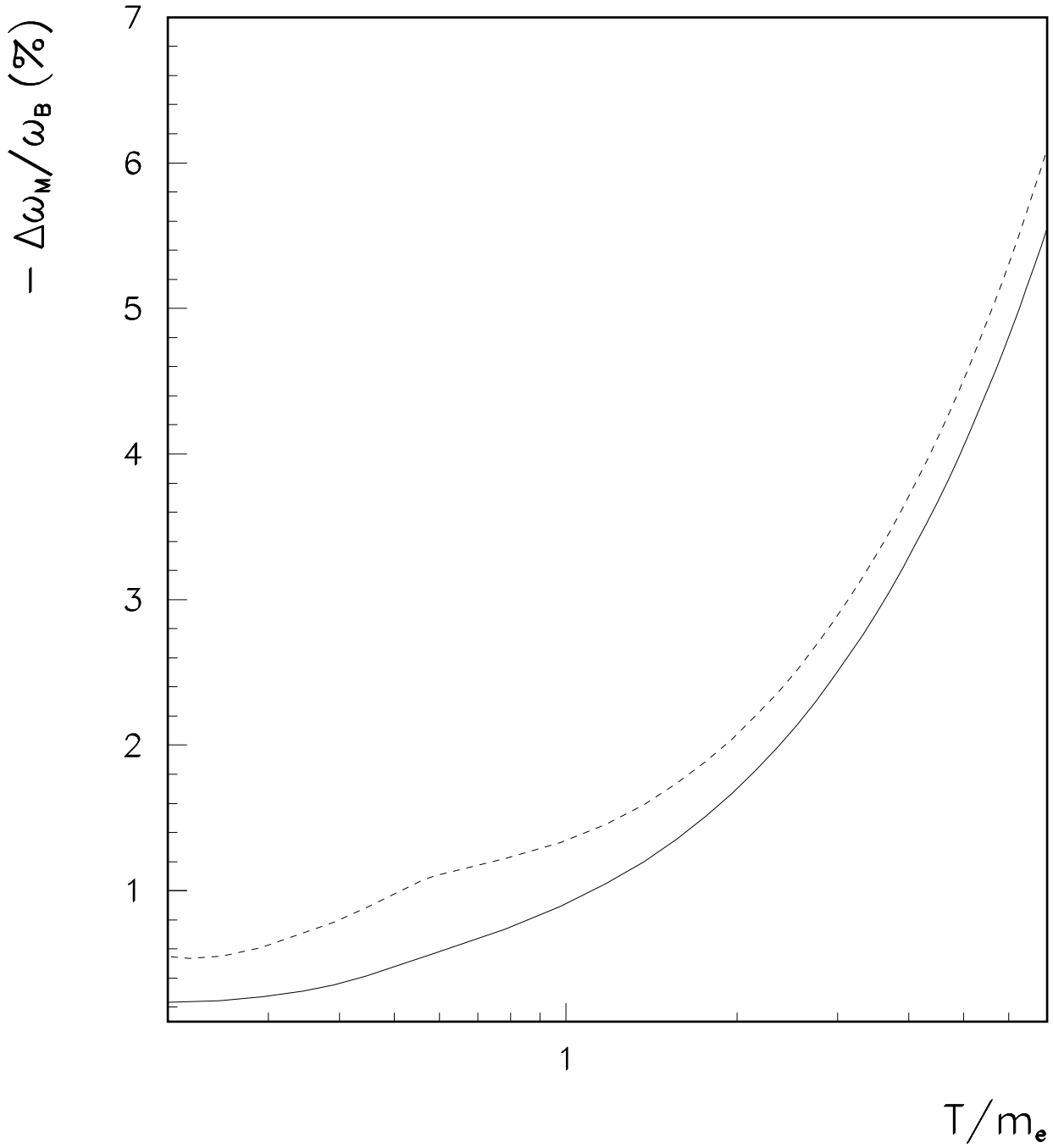


Figure 3: The finite nucleon mass corrections to Born rates, $\Delta\omega_M/\omega_B$, for $n \leftrightarrow p$ transitions.

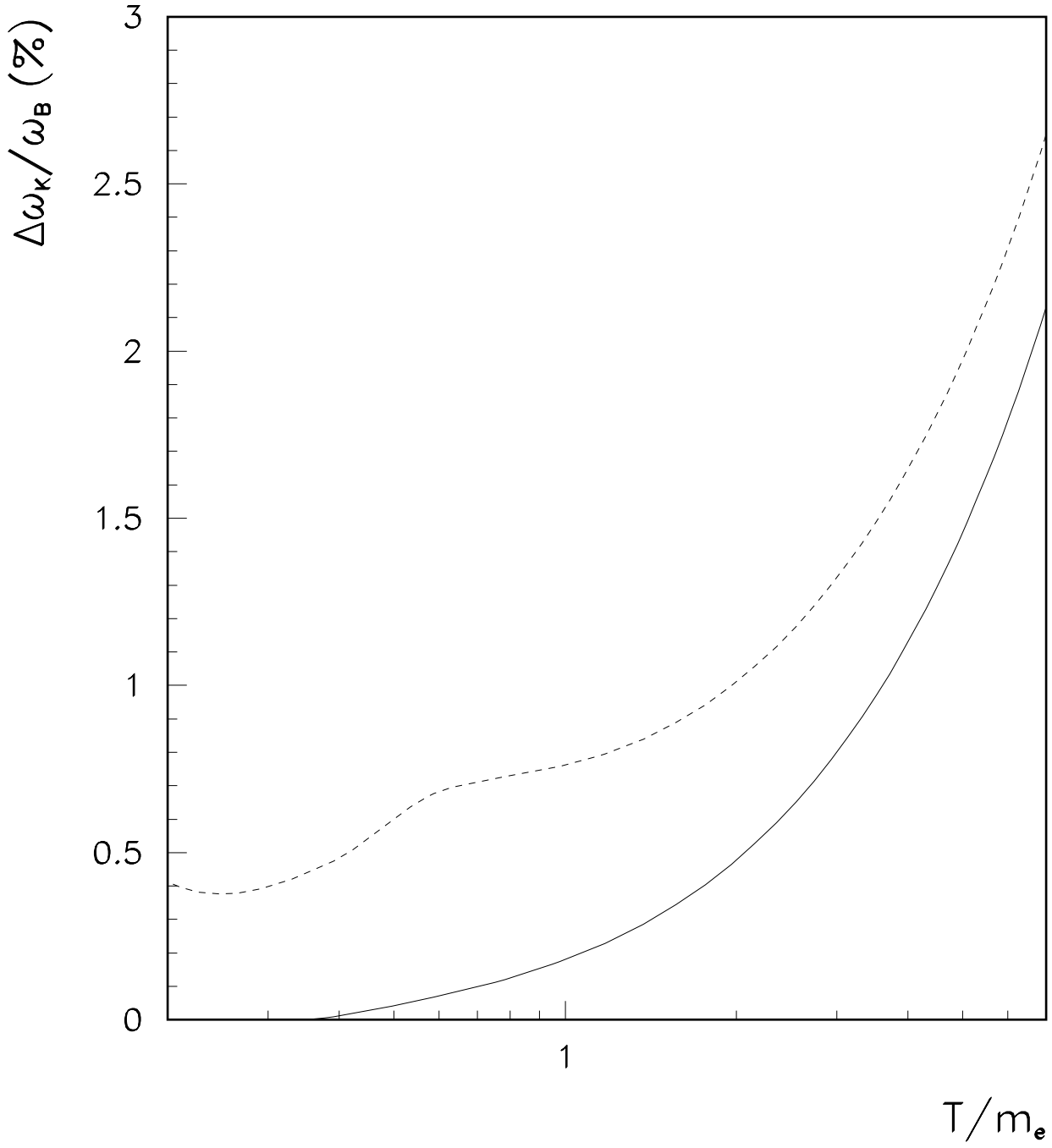


Figure 4: The *kinetic* corrections to Born rates, $\Delta\omega_K/\omega_B$, for $n \leftrightarrow p$ transitions.

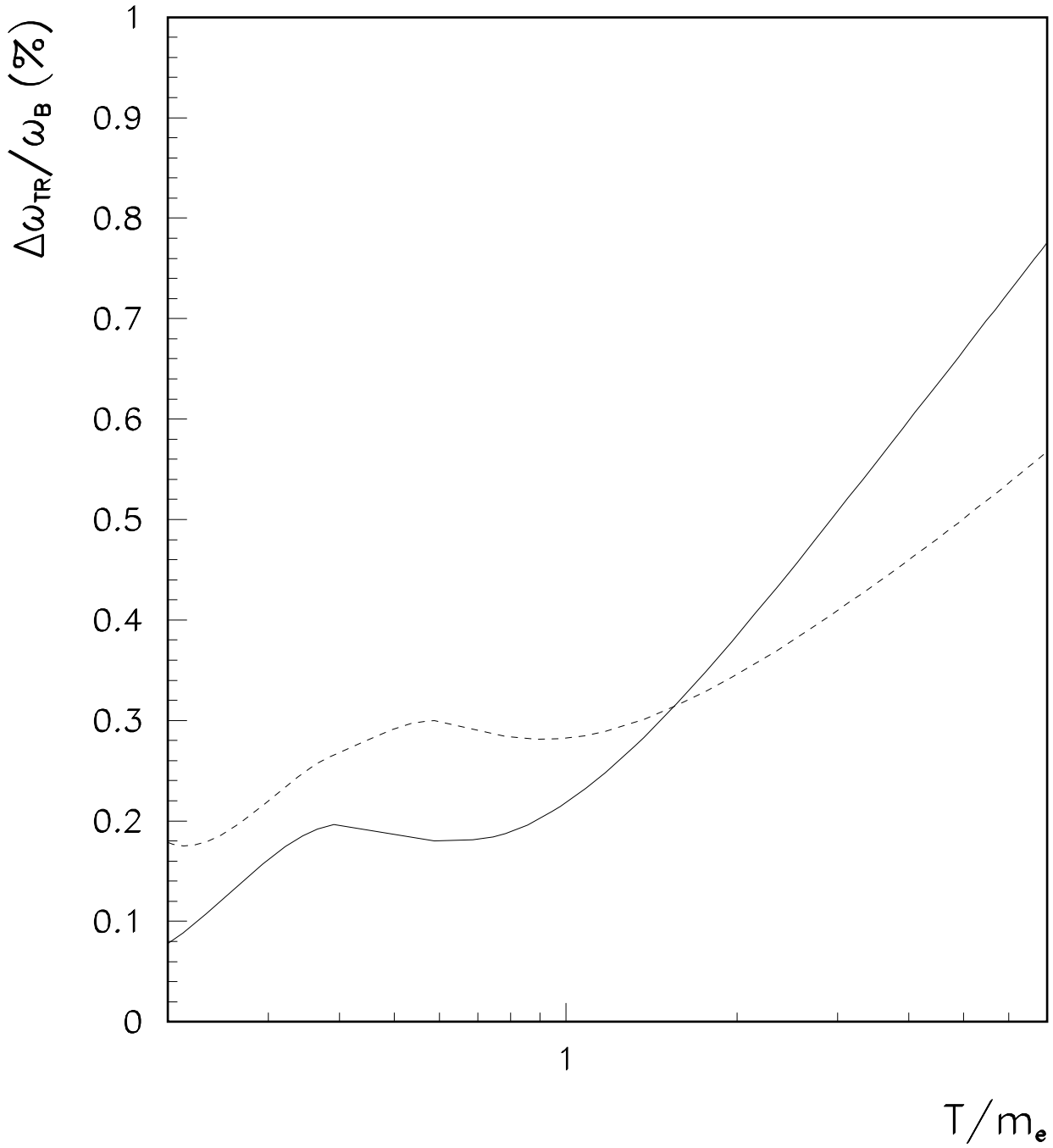


Figure 5: The thermal-radiative corrections to Born rates, $\Delta\omega_{TR}/\omega_B$, for $n \leftrightarrow p$ transitions.

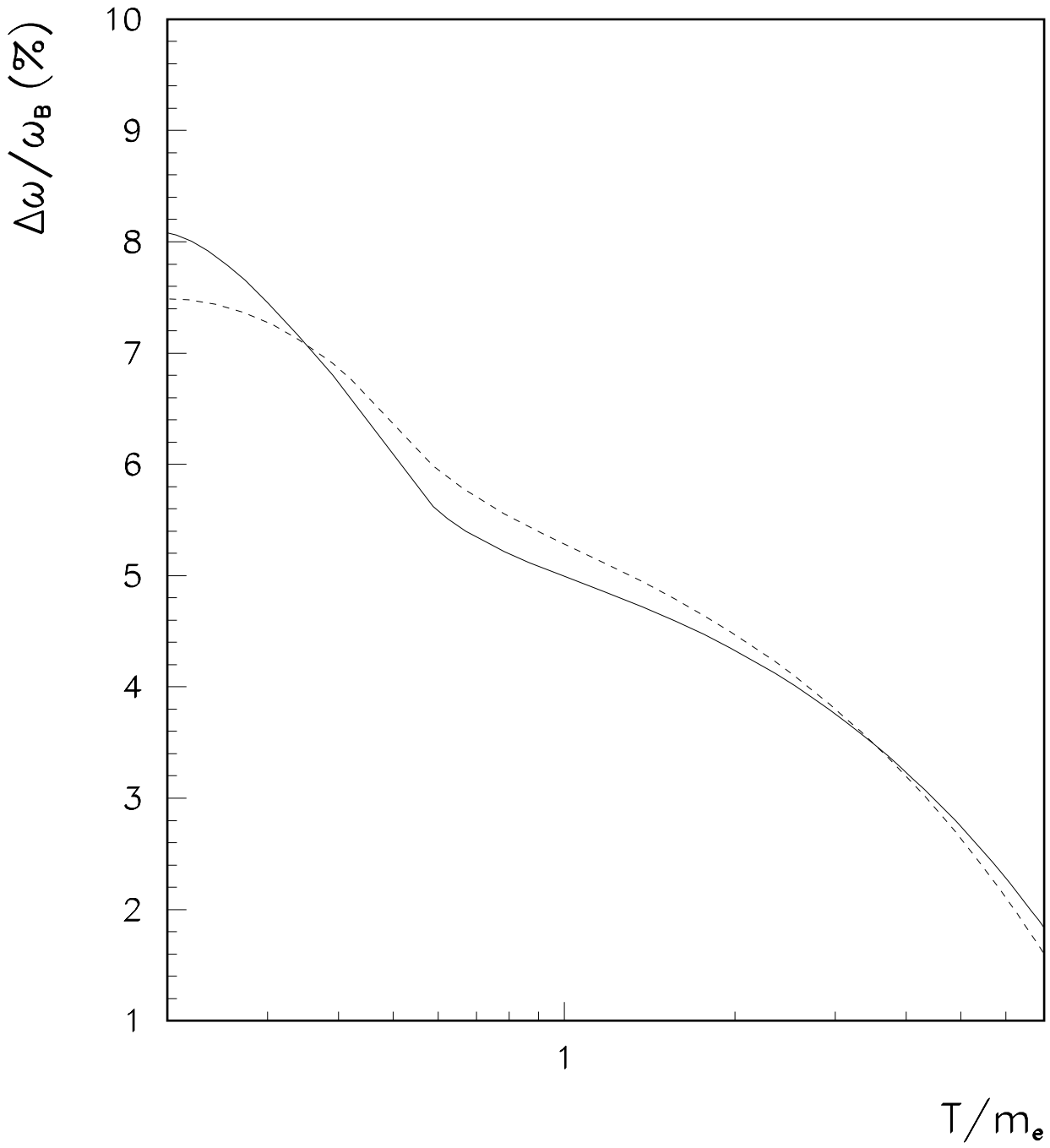


Figure 6: The total corrections to Born rates for $n \leftrightarrow p$ transitions.

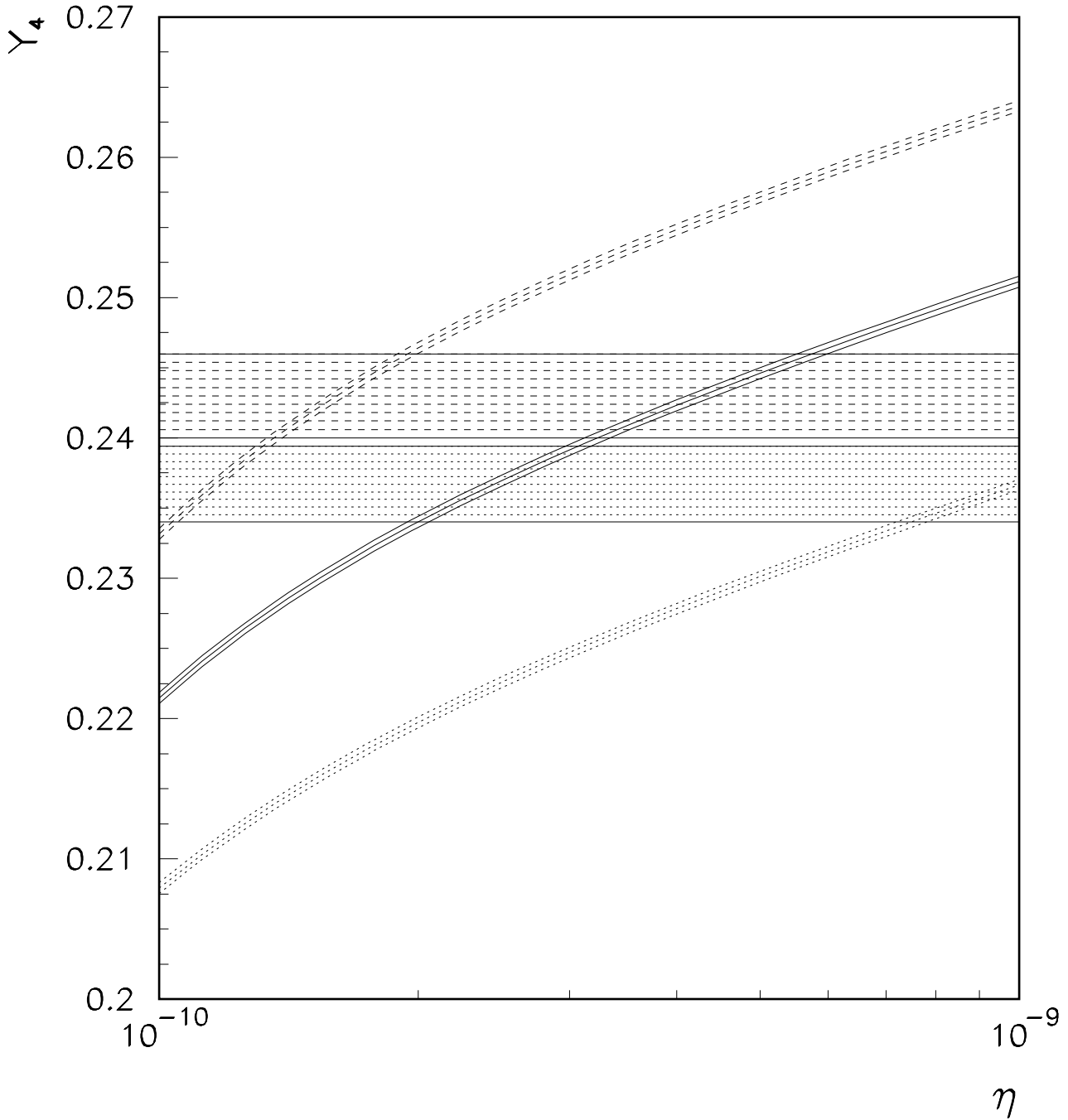


Figure 7: The ${}^4\text{He}$ mass fraction, Y_4 , versus η . The three solid lines are, from larger to lower values of Y_4 , the predictions corresponding to $N_\nu = 3$ and $\tau_n^{ex} = 888.6$ s, 886.7 s, 884.8 s, respectively. Analogously, the dashed lines correspond to $N_\nu = 4$ and the dotted ones to $N_\nu = 2$. The dotted and dashed horizontal band are the experimental values of Ref.s [2] and [3], respectively, with 1σ interval.

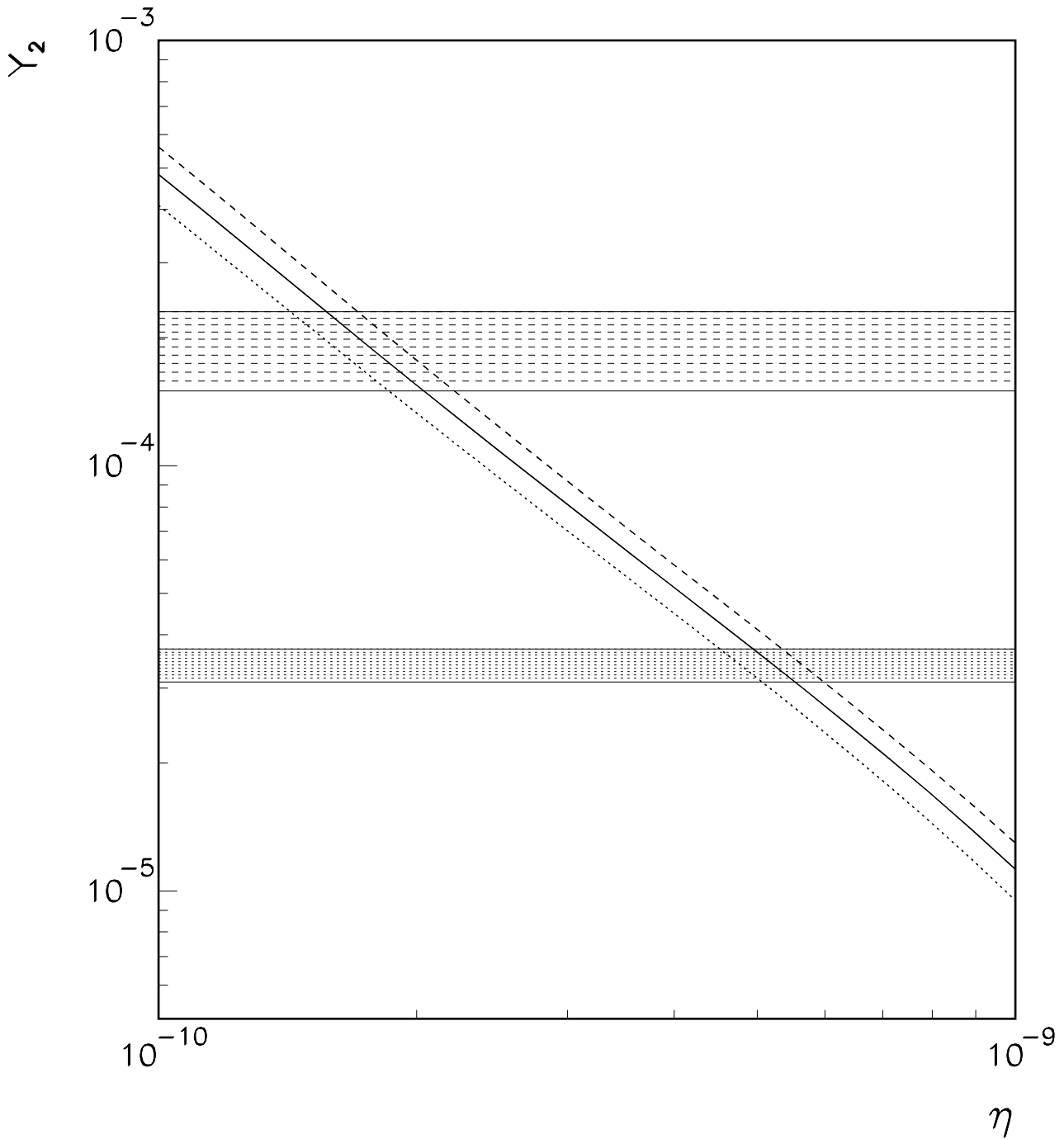


Figure 8: The quantity Y_2 versus η is reported. The notation used is the same of Fig. 8. Due to the negligible dependence of Y_2 on small variations of τ_n^{ex} no splitting of lines is present. The horizontal bands dashed and dotted are the experimental values of Ref.s [4, 5].

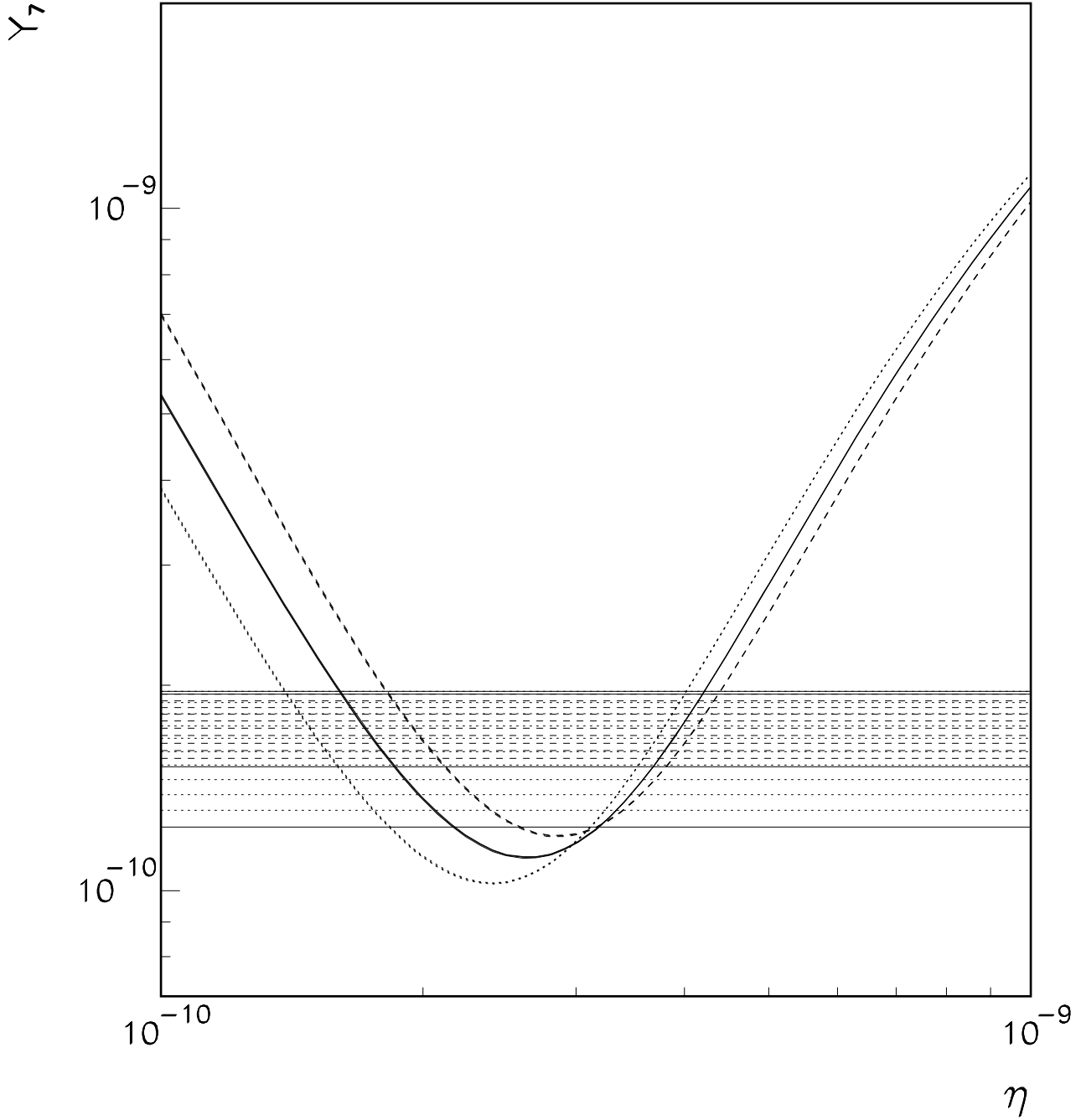


Figure 9: The quantity Y_7 versus η . The notation used is the same of Fig. 8. There is no splitting of lines related to $\Delta\tau_n$, due to the negligible dependence of Y_7 on small variations of τ_n^{ex} . The horizontal bands dashed and dotted are the experimental values of Ref.s [6, 7] and [9], respectively.

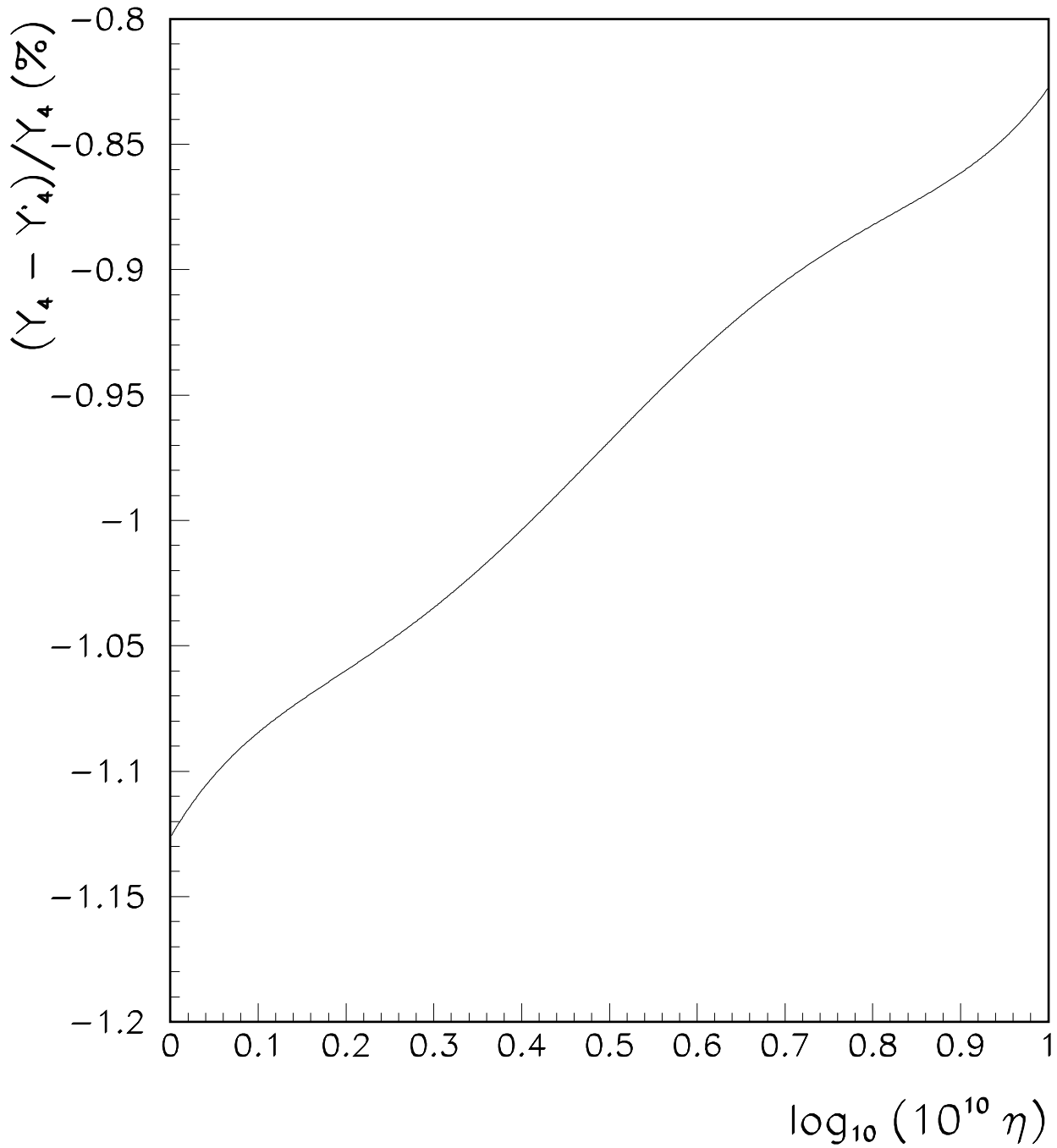


Figure 10: The ratio $(Y_4 - Y'_4)/Y_4$ versus $\log_{10}(10^{10}\eta)$ for $N_\nu = 3$ and $\tau_n = 885.3$ s [10] (see Section 5).

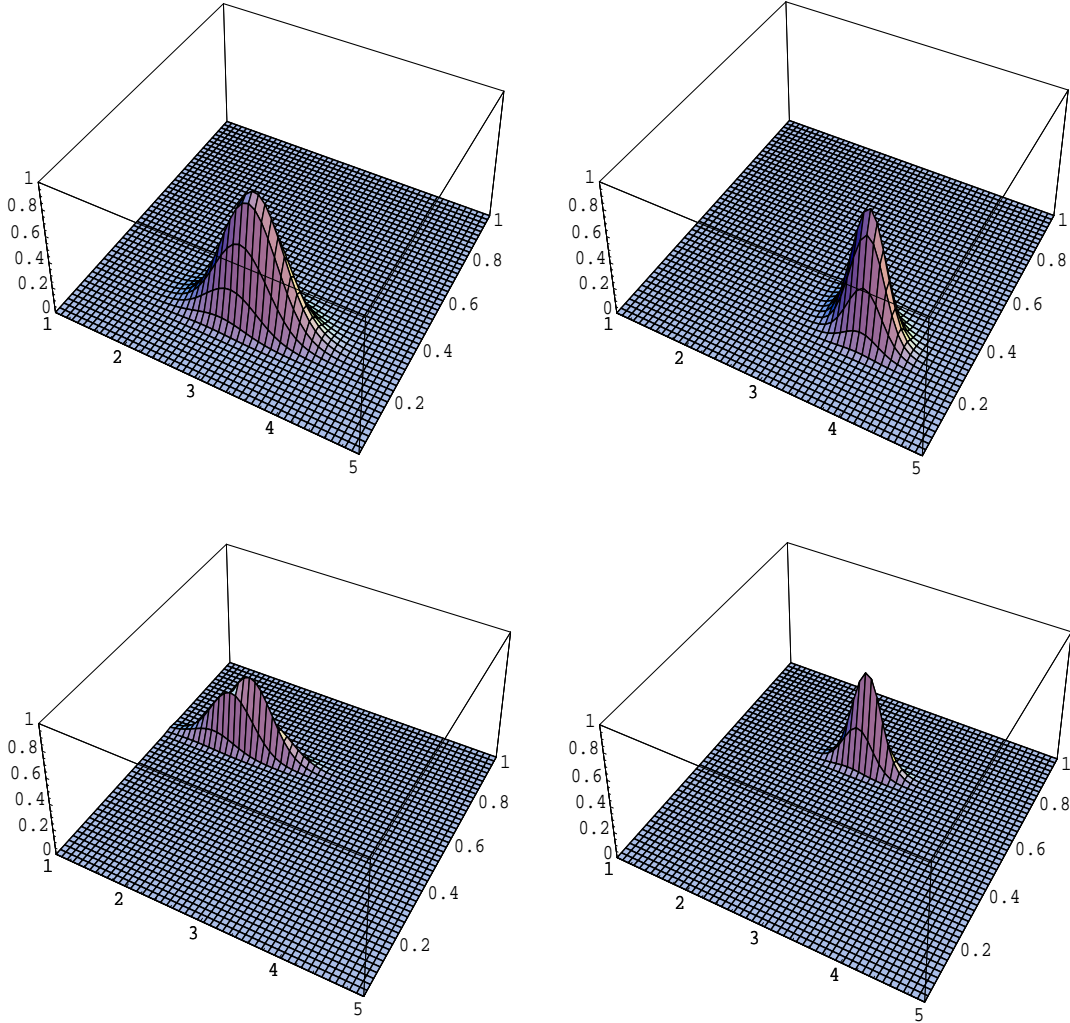


Figure 11: The likelihood distributions for the light element yields Y_2 , Y_4 , Y_7 are shown as functions of N_ν and $\log_{10}(10^{10})\eta$, normalized to unity in correspondence of the experimental values. From left to right and from top to bottom the following cases are considered: a) high D , low ${}^4\text{He}$; b) high D , high ${}^4\text{He}$; c) low D , low ${}^4\text{He}$; d) low D , high ${}^4\text{He}$. The plots for cases c) and d) are rescaled by a factor 25 and 100 times, respectively, compared to the one of a) and b).